PHYSICAL REVIEW D **83,** 023527 (2011)

New features in the curvaton model

Pravabati Chingangbam[*,†]

Astrophysical Research Center for the Structure and Evolution of the Cosmos, Sejong University, 98 Gunja Dong, Gwangjin gu, Seoul 143747, Korea

Qing-Guo Huang[‡]

Key Laboratory of Frontiers in Theoretical Physics, Institute of Theoretical Physics, Chinese Academy of Sciences, Beijing 100190, China

(Received 11 August 2010; published 27 January 2011)

We demonstrate novel features in the behavior of the second- and third-order nonlinearity parameters of the curvature perturbation, namely $f_{\rm NL}$ and $g_{\rm NL}$, arising from nonlinear motion of the curvaton field. We investigate two classes of potentials for the curvaton—the first has tiny oscillations superimposed upon the quadratic potential. The second is characterized by a single ''feature'' separating two quadratic regimes with different mass scales. The feature may either be a bump or a flattening of the potential. In the case of the oscillatory potential, we find that, as the width and height of superimposed oscillations increase, both $f_{\rm NL}$ and $g_{\rm NL}$ deviate strongly from their expected values from a quadratic potential. $f_{\rm NL}$ changes sign from positive to negative as the oscillations in the potential become more prominent. Hence, this model can be severely constrained by convincing evidence from observations that $f_{\rm NL}$ is positive. $g_{\rm NL}$, on the other hand, acquires very large negative values. Further, this model can give rise to a large running of $f_{\rm NL}$, with respect to scale. For the single-feature potential, we find that $f_{\rm NL}$ and $g_{\rm NL}$ exhibit oscillatory behavior as a function of the parameter that controls the feature. The running of $f_{\rm NL}$ with respect to scale is found to be small.

DOI: 10.1103/PhysRevD.83.023527 PACS numbers: 98.80.Cq

I. INTRODUCTION

The inflationary paradigm [1] has become an important ingredient of modern cosmology. Inflation provides a natural explanation for the production of the first density perturbations in the early Universe, which seeded the formation of the large-scale structure in the distribution of galaxies and the temperature anisotropies in the cosmic microwave background radiation [2]. However, the precise details of the mechanism for generating the primordial curvature perturbation are not fully established. The standard mechanism is via the quantum fluctuations of the inflaton field. An alternative scenario that frees the inflaton from the job of generating perturbations, besides giving rise to inflation, is the curvaton scenario [3–5]. In this scenario, an additional scalar field, called the *curvaton*, which is assumed to be very light, is invoked to generate the curvature perturbations. It is assumed to be frozen during inflation and begins evolving at the end of inflation. Its energy density is assumed to be subdominant during inflation, but it can share a significant part of the total energy in the Universe before its decay. The entropy perturbations caused by the curvaton field subsequently get converted into adiabatic perturbations.

A large number of light scalar fields are expected to be present in any fundamental theory that goes beyond the standard model of particle physics. During the inflationary era, these fields would have had the same amplitude of quantum fluctuations. It is plausible that at least some of them played important roles in the early Universe: for example, as the curvaton field. An important distinguishing property of the curvaton scenario as the generating mechanism for primordial perturbations, from the standard single slow-rolling field picture, is the possibility for the primordial perturbations to have large deviations from Gaussian distribution. This property becomes very attractive in the light of the recent result from WMAP that suggests that primordial non-Gaussianity may be large [6]. The non-Gaussianity generated in the curvaton scenario must have a local shape, because it is generated on superhorizon scales. Then, the curvature perturbation can be expanded at the same spatial point to nonlinear orders, as

$$\zeta(\mathbf{x}) = \zeta_g(\mathbf{x}) + \tfrac{3}{5} f_{\rm NL}[\zeta_g^2(\mathbf{x}) - \langle \zeta_g^2 \rangle] + \tfrac{9}{25} g_{\rm NL} \zeta_g^3(\mathbf{x}) + \ldots, \tag{1}$$

where $f_{\rm NL}$ and $g_{\rm NL}$ are the so-called non-Gaussianity parameters. The WMAP 7-yr result implies a constraint on the size of local form bispectrum, as $f_{\rm NL} = 32 \pm 21$ at the $1-\sigma$ level. The limits on $g_{\rm NL}$ are $-3.5 \times 10^5 < g_{\rm NL} < 8.2 \times 10^5$ (at a 95% confidence level) from the large-scale structure [7], and comparable limits are obtained from cosmic microwave background data from WMAP 5-yr data [8], as well. A convincing detection of the local form non-Gaussianity will rule out all single-field inflation in a model-independent way.

[*]Present address: Indian Institute of Astrophysics, Koramangala II Block, Bangalore 560034, India.
[†]prava@kias.re.kr
[‡]huangqg@itp.ac.cn

In the simplest case, the curvaton potential is assumed to have a quadratic form, and the typical size of the bispectrum is bounded by the tensor-scalar ratio, as $f_{\rm NL} < 10^3 r^{1/4}$ [9]. Since the curvaton field evolves linearly in this case, the size of the trispectrum is linearly related to that of the bispectrum, as

$$g_{\rm NL} \simeq -\tfrac{10}{3} f_{\rm NL}. \tag{2}$$

There is, however, no reason for the above relation to hold, in general, from the viewpoint of fundamental theory, since the curvaton potential could be different from the quadratic form. Case-by-case studies of different curvaton potentials have been done in the literature. These studies have focused on potentials that deviate from the quadratic form at large field values but tend to the quadratic form at small field values. The predictions of such models, particularly the level of non-Gaussianity, are then compared with those from the quadratic potential so as to understand their distinguishing features. Clearly, the distinctions become more prominent for large initial curvaton-field values. A distinct signature of departure of the curvaton potential from the quadratic form is a breakdown of the relation (2). If the curvaton self-interaction term becomes dominant, giving rise to higher-order corrections in the curvaton potential, the order of magnitude of $g_{\rm NL}$ can be $\mathcal{O}(f_{\rm NL}^2)$ [10–13]. The predictions for models with nearly quadratic potential are investigated in [14–17], where the nonlinear evolution of the curvaton after inflation but prior to its oscillation is taken into account. Another promising curvaton candidate is the pseudo-Nambu-Goldstone boson-axion, whose potential significantly deviates from the quadratic form around the top of its potential. A numerical analysis of the axion-type curvaton model is discussed in [18,19]. From the viewpoint of fundamental theory, one can generically expect multicurvaton models, and such a model is investigated in [20,21]. While the discussion, thus far, has ignored the scale dependence of the bispectrum and the trispectrum, it is possible that, in the future, such scale dependence may become accessible to experimental observation and, hence, important [22–25]. The scale dependence of $f_{\rm NL}$ can be quantified by its spectral index, $n_{f_{\rm NL}}$, which is defined by

$$f_{\rm NL}(k) = f_{\rm NL}(k_p)\left(\frac{k}{k_p}\right)^{n_{f_{\rm NL}}}, \tag{3}$$

where k_p is some suitable pivot scale. The forecast of $1-\sigma$ uncertainty for $n_{f_{\rm NL}}$ that can be reached by Planck [26] and CMBPol [27] for the local form bispectrum is as follows [28]:

$$\Delta n_{f_{\rm NL}} \simeq 0.1 \frac{50}{f_{\rm NL}} \frac{1}{\sqrt{f_{\rm sky}}} \quad \text{for Planck,} \tag{4}$$

and

$$\Delta n_{f_{\rm NL}} \simeq 0.05 \frac{50}{f_{\rm NL}} \frac{1}{\sqrt{f_{\rm sky}}} \quad \text{for CMBPol,} \tag{5}$$

where $f_{\rm sky}$ is the sky fraction. Other relevant papers are [29–34].

In this paper, we discuss two new curvaton models that are different from the ones described above. The first is a potential that has tiny oscillations superimposed on the quadratic form. Such oscillatory corrections could arise, for example, if we consider instanton corrections to the potential of the Goldstone boson with a shift symmetry. The curvaton experiences the small bumps of the oscillations in the potentials as it undergoes oscillations about the minimum of the potential. As a consequence, the curvaton evolution during this stage is nonlinear (the curvaton equation of motion is not that of a damped simple harmonic oscillator), making it significantly different from the case of the quadratic potential. Our goal is to calculate the nonlinear curvature perturbation up to cubic order and obtain the predictions for non-Gaussianity from such a model. We find very interesting new implications for the nonlinearity parameters $f_{\rm NL}$ and $g_{\rm NL}$ arising in this model. First, $f_{\rm NL}$ is no longer restricted to have positive values. Depending on the amplitude and the frequency of the superimposed oscillations on the potential, it can take a wide range of both positive and negative, with a switch of sign from positive to negative. $g_{\rm NL}$, on the other hand, remains negative and can take large negative values. The sign switch of $f_{\rm NL}$ brings up the possibility that the most important contribution to primordial non-Gaussianity could come from the $g_{\rm NL}$ term, with $f_{\rm NL}$ being negligibly small.

The second model we discuss is a class of potentials characterized by a single *feature* separating two quadratic regimes with different mass scales. The feature depends on a single parameter, and, depending on the sign of the parameter, it can be either a single bump or a flattening of the slope of the quadratic potential at some characteristic scale. Such features in the scalar-field potentials are expected in supergravity theories and have been studied in the context of inflaton perturbations [35]. We find that the effect of the feature on $f_{\rm NL}$ and $g_{\rm NL}$ is rather dramatic, causing them to oscillate with increasing amplitude as the strength of the feature increases.

This paper is organized as follows: in Sec. II, we briefly summarize the method for computation of the nonlinear curvature perturbation using the δN formalism and the curvaton equation of motion. In Sec. III, we describe the specific forms of the curvaton potentials we are considering here and display our results for the nonlinear corrections to the curvature perturbations. In Sec. III A, we discuss the case of the washboard potential, while in Sec. III B, we discuss the single-feature potential. We end with a summary of our results and comments in Sec. IV. A brief description of the curvaton with quadratic potential is given in the Appendix to highlight the differences from our study and the novelty of our results.

II. THE NONLINEAR CURVATURE PERTURBATION

On sufficiently large scales, the curvature perturbation on the uniform density slicing can be calculated by using the so-called δN formalism [36–40]. Starting from any initial flat slice at time $t_{\rm ini}$, on the uniform density slicing, the curvature perturbation is

$$\zeta(t, \mathbf{x}) = \delta N \equiv N(t, \mathbf{x}) - N_0(t), \tag{6}$$

where $N(t, \mathbf{x}) = \ln a(t, \mathbf{x})/a(t_{\rm ini})$ describes the local expansion of our Universe, and $N_0(t) = \ln a(t)/a(t_{\rm ini})$ is the unperturbed amount of expansion. In the curvaton model, the difference between local expansion and the unperturbed expansion is caused by the quantum fluctuations of the curvaton field during inflation. Therefore,

$$\zeta = N_{,\sigma}\delta\sigma + \tfrac{1}{2}N_{,\sigma\sigma}\delta\sigma^2 + \tfrac{1}{6}N_{,\sigma\sigma\sigma}\delta\sigma^3 + \ldots, \tag{7}$$

where $N_{,\sigma} = dN/d\sigma$, $N_{,\sigma\sigma} = d^2N/d\sigma^2$, and $N_{,\sigma\sigma\sigma} = d^3N/d\sigma^3$. Considering $\delta\sigma = H_*/2\pi$, the amplitude of the power spectrum generated by the curvaton is

$$P_{\zeta_\sigma} = N_{,\sigma}^2\left(\frac{H_*}{2\pi}\right)^2, \tag{8}$$

and the non-Gaussianity parameters are given by

$$f_{\rm NL} = \frac{5}{6}\frac{N_{,\sigma\sigma}}{N_{,\sigma}^2}, \tag{9}$$

$$g_{\rm NL} = \frac{25}{54}\frac{N_{,\sigma\sigma\sigma}}{N_{,\sigma}^3}, \tag{10}$$

where H_* is the Hubble parameter during inflation. At third-order perturbation, there is actually one more parameter, $\tau_{\rm NL}$, which measures another aspect of the local form trispectrum. However, when the curvature perturbation is only produced by the curvaton field, $\tau_{\rm NL}$ is not an independent parameter, and it is related to $f_{\rm NL}$ by

$$\tau_{\rm NL} = (\tfrac{6}{5}f_{\rm NL})^2. \tag{11}$$

The amplitude of the tensor perturbation depends only on the inflation scale, as

$$P_T = \frac{H_*^2/M_p^2}{\pi^2/2}. \tag{12}$$

Thus, the tensor-scalar ratio r is given by

$$r \equiv P_T/P_{\zeta_\sigma} = \frac{8}{N_{,\sigma}^2 M_p^2}. \tag{13}$$

In this work, we consider the simplest version of the curvaton scenario, where only the quantum fluctuations of the curvaton field contribute to the total curvature perturbation.

After inflation, the equations of motion are

$$H^2 = \frac{1}{3M_p^2}(\rho_r + \rho_\sigma), \tag{14}$$

$$\dot\rho_r + 4H\rho_r = 0, \tag{15}$$

$$\rho_\sigma = \tfrac{1}{2}\dot\sigma^2 + V(\sigma), \tag{16}$$

$$\ddot\sigma + 3H\dot\sigma + \frac{dV(\sigma)}{d\sigma} = 0, \tag{17}$$

where ρ_r and ρ_σ are the energy densities of the radiation and the curvaton, respectively, and $V(\sigma)$ is the curvaton potential. In order to numerically solve the above differential equations, we define the reduced curvaton field $\tilde\sigma$ and the reduced curvaton potential $V(\tilde\sigma)$ as follows:

$$\tilde\sigma = \sigma/\sigma_*, \tag{18}$$

$$V(\tilde\sigma) = \frac{V(\sigma)}{m^2\sigma_*^2}, \tag{19}$$

where σ_* is the vacuum expectation value of the curvaton field in the inflationary era. The equations of motion can be simplified as

$$N' = \left[\alpha e^{-4N} + \frac{\sigma_*^2}{3M_p^2}\left\{\frac{1}{2}\tilde\sigma'^2 + V(\tilde\sigma)\right\}\right]^{1/2}, \tag{20}$$

$$\tilde\sigma'' + 3N'\tilde\sigma' + \frac{dV(\tilde\sigma)}{d\tilde\sigma} = 0, \tag{21}$$

where $N(x) = \ln a(t)$, $\alpha = \frac{\rho_{r,\rm ini}}{3M_p^2m^2} = H_{\rm ini}^2/m^2$, the prime denotes the derivative with respect to the dimensionless time coordinate $x \equiv mt$, and the Hubble parameter becomes

$$H = mN'. \tag{22}$$

The solution for the subdominant curvaton with quadratic potential is analytically discussed in the Appendix.

Using the reduced curvaton field $\tilde\sigma$, the non-Gaussianity parameters are given by

$$f_{\rm NL} = \frac{5}{6}\frac{N_{,\tilde\sigma\tilde\sigma}}{N_{,\tilde\sigma}^2}, \tag{23}$$

$$g_{\rm NL} = \frac{5}{6}\frac{N_{,\tilde\sigma\tilde\sigma\tilde\sigma}}{N_{,\tilde\sigma}^3}. \tag{24}$$

Quoting the formula in [23–25], the spectral index of $f_{\rm NL}$ is given by

$$n_{f_{\rm NL}} = \tilde\eta_3\frac{N_{,\tilde\sigma}}{N_{,\tilde\sigma\tilde\sigma}}, \tag{25}$$

where

$$\tilde\eta_3 = \eta_{mm}V'''(\tilde\sigma)|_{\tilde\sigma=1}, \tag{26}$$

$\eta_{mm} = m^2/3H_*^2$, and $V'''(\tilde\sigma) = d^3V(\tilde\sigma)/d\tilde\sigma^3$. Since $\tau_{\rm NL} = (\frac{6}{5}f_{\rm NL})^2$, we obtain $n_{\tau_{\rm NL}} = 2n_{f_{\rm NL}}$. In this paper, we will

show our results in terms of the rescaled variable $n_{f_{\rm NL}} f_{\rm NL}/\eta_{mm}$, which is given by

$$\frac{n_{f_{\rm NL}} f_{\rm NL}}{\eta_{mm}} = \frac{5}{6N_{,\tilde{\sigma}}} V'''(\tilde{\sigma})|_{\tilde{\sigma}=1}. \quad (27)$$

Note that, for the quadratic potential, $f_{\rm NL}$ is exactly scale-invariant.

The scale factor can be rescaled to satisfy $a(t_{\rm ini}) = 1$, or equivalently $N(t_{\rm ini}) = 0$. For numerical calculation, we also need to input the value of α. If the vacuum energy of the inflaton suddenly decays into radiation, a reasonable choice is $\alpha = H_{\rm inf}^2/m^2$, which is much larger than 1. However, we do not know its exact value. But as long as α is large enough, it does not affect our numerical result, because the curvaton field almost does not move when the Hubble parameter is much larger than its mass. For example, it is reasonable to assume that the Hubble parameter at the inflationary era is at least 1 order of magnitude larger than the curvaton mass, and then we set $\alpha = 10^2$ in this paper.

III. THE MODELS

In this section, we consider two new curvaton models, which have some small features around the exactly quadratic form of the curvaton potential. We can expect that these features will introduce nonlinear effects to the oscillating curvaton field and, consequently, affect the non-Gaussianity parameters. Our aim is to calculate these precise effects. Note that these effects are different from what was considered in [14–17], where the nonlinear evolution of the curvaton after inflation but prior to its oscillation was considered. Since the nonlinear nature of the curvaton motion makes analytic solutions extremely difficult to obtain, we rely on numerical methods to get our results. We solve Eqs. (20) and (21) as a coupled set of differential equations for each potential under consideration.

A. Washboard curvaton model

A good candidate for the curvaton is the Goldstone boson with shift symmetries $\sigma \to \sigma + \delta$ [18,19]. Considering the instanton correction, the potential of σ can be written as

$$V(\sigma) = \Lambda^4\left(1 - \cos\frac{\sigma}{f}\right) + \tilde{\Lambda}^4\left(1 - \cos\frac{\sigma}{f/n}\right) + \ldots, \quad (28)$$

where n is an integer. Usually, the scale $\tilde{\Lambda}$ is suppressed by a UV scale $M(\gg \Lambda)$, compared to Λ, and then, the second term is taken as a small correction to the potential. For a large n and $\sigma \ll f$, the above potential can be expressed by

$$V(\sigma) = \frac{1}{2}m^2\sigma^2 + V_0\left[1 - \cos\left(\frac{\sigma}{F}\right)\right], \quad (29)$$

where $V_0 \ll V_* = \frac{1}{2}m^2\sigma_*^2$. We call it the *washboard potential*. The potential expressed in terms of $\tilde{\sigma}$ is

$$V(\tilde{\sigma}) = \tfrac{1}{2}\tilde{\sigma}^2 + \epsilon[1 - \cos(\tilde{\sigma}/\delta)], \quad (30)$$

where

$$\epsilon = \frac{V_0}{m^2\sigma_*^2}, \qquad \delta = \frac{F}{\sigma_*}. \quad (31)$$

ϵ measures the size of the correction, and δ characterizes the period of oscillation of the correction term in Eq. (30). The reduced potential is shown in the left panel of Fig. 1 for easy visualization. Note that when $\tilde{\sigma} \gg \sqrt{\epsilon}$, the potential is almost quadratic. If $\tilde{\sigma} \ll \delta$, then $V(\tilde{\sigma}) \simeq \frac{1}{2}(1 + \epsilon/\delta^2)\tilde{\sigma}^2$, which is roughly quadratic but with a deformed mass.

The dynamics of the curvaton field after inflation are governed by

$$\tilde{\sigma}'' + \frac{3}{2x}\tilde{\sigma}' + \tilde{\sigma} + \frac{\epsilon}{\delta}\sin(\tilde{\sigma}/\delta) = 0. \quad (32)$$

Even though the correction to the potential is small, the curvaton-field dynamics can become significantly

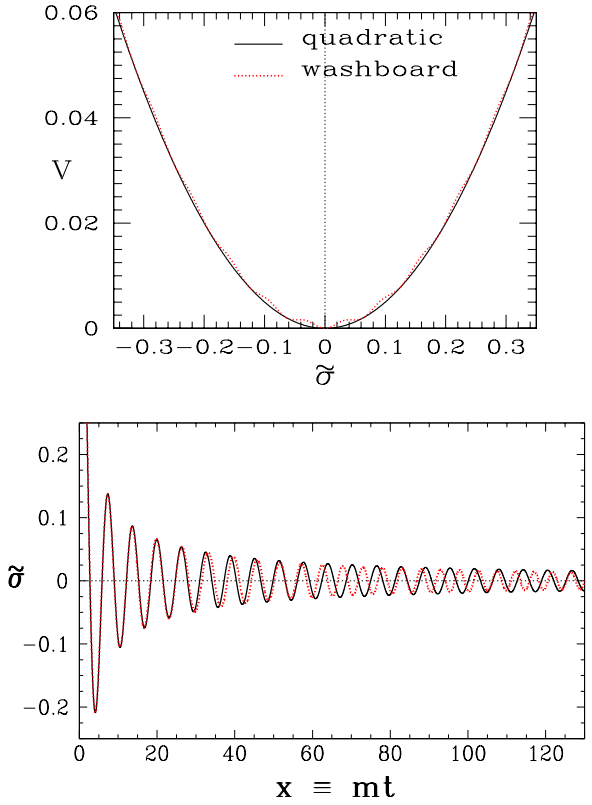

FIG. 1 (color online). The washboard curvaton potential given by Eq. (29) is shown on the top panel for visual comparison with the corresponding quadratic one. The parameter values are $\epsilon = 5 \times 10^{-4}$ and $\delta = 10^{-2}$. We have chosen a large value of ϵ in order to make the oscillations clearly visible. The bottom panel shows the curvaton oscillations about the potential minimum for the quadratic and washboard cases, with the same initial field value given by $\sigma_*/M_p = 0.1$. The parameter values for this plot are $\epsilon = 10^{-4}$ and $\delta = 10^{-2}$.

nonlinear, provided the period of the correction term is small enough. We consider, here, the situation where the dynamics of the curvaton are dominated by the mass term at the commencement of its evolution. This implies that $\epsilon/\delta < 1$. Once the amplitude of the curvaton oscillation drops below ϵ/δ, the curvaton evolves nonlinearly. On the right panel of Fig. 1, we have plotted the oscillation of the curvaton field about the minimum of the potential for the quadratic and the washboard potential cases, for the same initial field value given by $\sigma_*/M_p = 0.1$. We can see that the amplitude of oscillation in the washboard case decreases faster than the quadratic case. Moreover, the frequency of oscillation for the washboard curvaton is time-dependent, as it oscillates about the constant frequency of the quadratic case.

We now illustrate how the small features in the curvaton potential play an important role for the non-Gaussianity parameters. We solve for $N_{,\sigma}$, $N_{,\sigma\sigma}$, and $N_{,\sigma\sigma\sigma}$ and then obtain $f_{\rm NL}$ and $g_{\rm NL}$ from them. In general, we need to scan four independent parameters—namely, Γ/m, σ_*/M_p, ϵ, and δ—in order to satisfy observational constraints such as the amplitude of perturbations and the limits on $f_{\rm NL}$ and $g_{\rm NL}$. Our strategy, here, is to fix Γ/m, σ_*/M_p, and δ and obtain $f_{\rm NL}$ and $g_{\rm NL}$ as functions of ϵ. Our results are obtained for two values of Γ/m and δ each, to understand how these parameters systematically affect $f_{\rm NL}$ and $g_{\rm NL}$. It must be mentioned that, for the quadratic potential, Γ/m is typically required to be of the order of 10^{-8} for the amplitude of perturbations to be COBE normalized. Evolving the equations numerically until the energy density of the curvaton decreases to such a small value is prohibitively time consuming. Moreover, for the purpose of capturing the essential features of the dependence of $f_{\rm NL}$ and $g_{\rm NL}$ on ϵ and δ, it is enough to fix Γ/m at a relatively large value.

In Fig. 2, we have plotted $f_{\rm NL}$, $g_{\rm NL}$, and $n_{f_{\rm NL}} f_{\rm NL}/\eta_{mm}$ as functions of ϵ, for $\Gamma/m = 10^{-2}$ and 2×10^{-2} and fixed values of $\delta = 10^{-2}$ and $\sigma_*/M_p = 0.1$. We can see that Γ/m systematically changes the amplitudes of $f_{\rm NL}$ and $g_{\rm NL}$, but does not alter the essential functional shapes. The correctness of the numerical calculations is tested by ensuring that, in the limit $\epsilon \to 0$, $f_{\rm NL}$ and $g_{\rm NL}$ tend to their analytically expected values for the quadratic potential, as clearly seen in the figure. As ϵ increases, $f_{\rm NL}$ and $g_{\rm NL}$ become strongly affected and deviate from their expectation from the quadratic potential. $f_{\rm NL}$ crosses over from positive to increasingly negative values as ϵ increases. On the other hand, $g_{\rm NL}$ remains negative throughout, but its magnitude becomes very large as ϵ increases. The inset in the middle panel of Fig. 2, which shows $g_{\rm NL}$, zooms in to the $\epsilon \to 0$ region to show it approaching the negative value expected from the quadratic potential. The bottom panel demonstrates that this model can have a large running of $f_{\rm NL}$. $n_{f_{\rm NL}} f_{\rm NL}/\eta_{mm}$ grows linearly with ϵ.

Next, in Fig. 3, we have plotted $f_{\rm NL}$, $g_{\rm NL}$, and $n_{f_{\rm NL}} f_{\rm NL}/\eta_{mm}$ for two different values of δ. We have

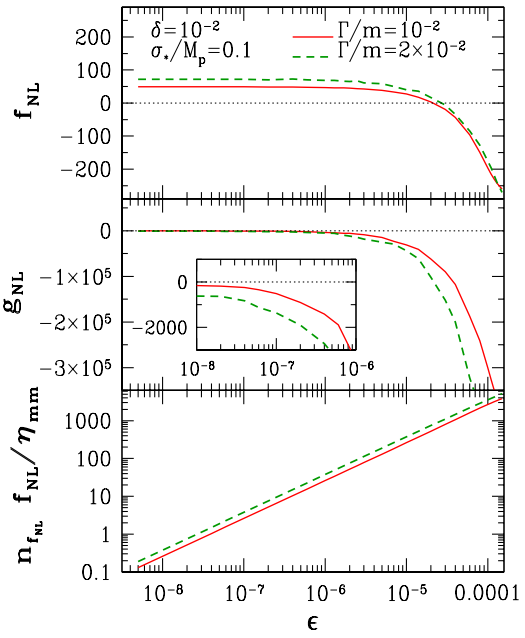

FIG. 2 (color online). $f_{\rm NL}$, $g_{\rm NL}$, and $n_{f_{\rm NL}} f_{\rm NL}/\eta_{mm}$ are shown as functions of ϵ for the washboard potential, for fixed values of δ, Γ/m, and σ_*/M_p. We have shown plots for two different values of Γ/m in order to demonstrate the systematic variation as we change Γ/m.

chosen $\delta = 10^{-2}$ and 1.8×10^{-2} and fixed $\Gamma/m = 10^{-2}$ and $\sigma_*/M_p = 0.1$. We see that, for very small ϵ, varying δ has little effect on the behavior of $f_{\rm NL}$ and $g_{\rm NL}$. This can be explained by the fact that $\epsilon \to 0$ kills off the oscillations superimposed on the potential, regardless of the frequency of oscillations that is controlled by δ. At relatively larger

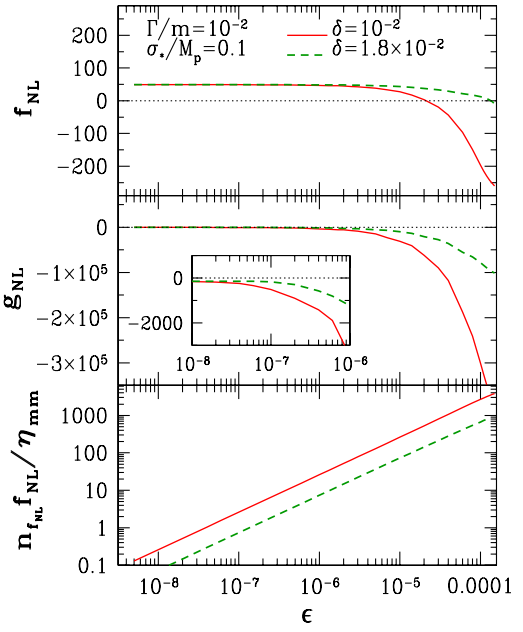

FIG. 3 (color online). Same as Fig. 2, but for two different values of δ, with Γ/m and σ_*/M_p kept fixed.

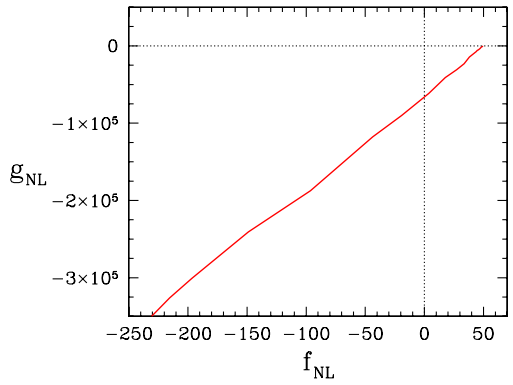

FIG. 4 (color online). $g_{\rm NL}$ versus $f_{\rm NL}$ at different values of ϵ for the washboard potential. The other parameter values are $\Gamma/m = 10^{-2}$, $\sigma_*/M_p = 0.1$, and $\delta = 10^{-2}$.

values of ϵ, the effect of δ becomes prominent. The deviation of $f_{\rm NL}$ and $g_{\rm NL}$ from the quadratic potential behavior increases as δ decreases, due to the increase in the frequency of the oscillations in the potential.

In Fig. 4, we have plotted $g_{\rm NL}$ versus $f_{\rm NL}$ at different values of ϵ. The parameter values are $\Gamma/m = 10^{-2}$, $\sigma_*/M_p = 0.1$, and $\delta = 10^{-2}$. As can be seen from the figure, the relation between $g_{\rm NL}$ versus $f_{\rm NL}$ is roughly linear with positive slope. In comparison, the quadratic case has negative slope.

B. Single-feature curvaton model

Some features are expected in the scalar-field potential from the supergravity theories [35]. In this subsection, we are interested in how these features affect the non-Gaussianity parameters in the curvaton model. For simplicity, we parametrize the curvaton potential with a feature as follows:

$$V(\sigma) = \frac{1}{2}m^2\sigma^2\left[1 + \frac{c}{1 + (\sigma/M)^{2n}}\right], \tag{33}$$

where $n > 0$, and M is an energy scale that measures the position of the feature. In the regime $\sigma \gg M$ or $\sigma \ll M$, the curvaton potential has a quadratic form, but, around $\sigma \sim M$, the potential deviates from the quadratic form. As in the previous subsection, we define a reduced potential as follows:

$$V(\tilde{\sigma}) = \frac{1}{2}\tilde{\sigma}^2\left[1 + \frac{c}{1 + (\tilde{\sigma}/d)^{2n}}\right], \tag{34}$$

where

$$d = \frac{M}{\sigma_*}. \tag{35}$$

The reduced potential given by Eq. (34) is shown in Fig. 5 for $n = 2$ and $d = 0.1$. The nature of the feature depends on the sign of c. If c is positive, then there is a bump, whereas a negative c changes the slope of the potential to make it flatter around some scale set by the parameter d.

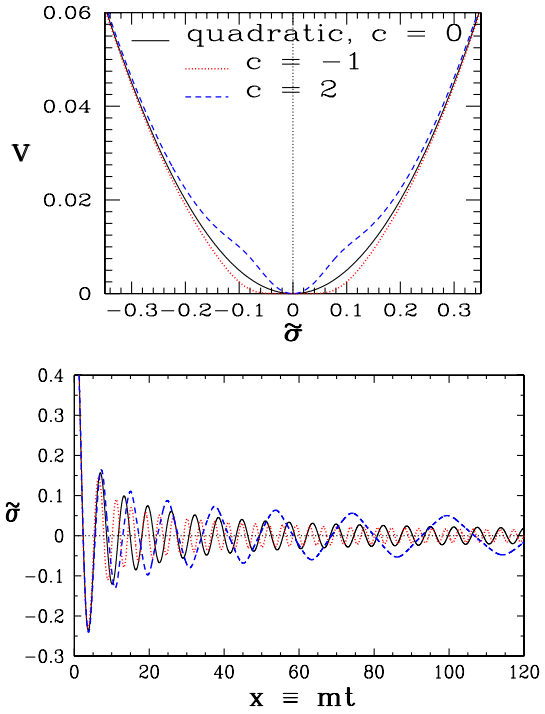

FIG. 5 (color online). The single-feature curvaton potential given by Eq. (34) is shown on the left panel for comparison with the corresponding quadratic one. d is fixed to be 0.1, and we have plotted for $c = 2$ and -1 to show how the nature of the feature changes with the sign of c. The right panel shows the corresponding curvaton oscillations about the potential minimum, with the same initial field value given by $\sigma_*/M_p = 0.1$.

The equation of motion for the reduced curvaton field becomes

$$\tilde{\sigma}'' + 3N'\tilde{\sigma}' + \left\{1 + c\frac{1 - (n-1)(\tilde{\sigma}/d)^{2n}}{[1 + (\tilde{\sigma}/d)^{2n}]^2}\right\}\tilde{\sigma} = 0. \tag{36}$$

We restrict our analysis, here, to $n = 2$. If $d \ll 1$, and the initial curvaton-field value is large enough, then the curvaton evolves linearly prior to its oscillation. We choose $d = 0.1$. As in the washboard curvaton model, we choose Γ_σ/m to be 10^{-2}, and $\sigma_*/M_p = 10^{-1}$. Then, we solve for $f_{\rm NL}$, scanning the parameter c.

In Fig. 6, we show $f_{\rm NL}$ and $g_{\rm NL}$ for the single-feature potential. As seen in the figure, $f_{\rm NL}$ oscillates about zero with increasing amplitude as $|c|$ increases. It flattens out and approaches the expected value from the quadratic potential as $|c| \to 0$. $g_{\rm NL}$ also exhibits oscillatory behavior as c varies. Similar to $f_{\rm NL}$, we can see the curve flattening out near $c = 0$ and agreeing with the value expected from the quadratic potential (the inset in the bottom panel of the figure zooms in around $c = 0$). For this model, $n_{f_{\rm NL}} f_{\rm NL}/\eta_{mm} \sim -10cd^4$ and is much smaller than 1 in the parameter range considered here.

In Fig. 7, we have plotted $g_{\rm NL}$ versus $f_{\rm NL}$ at different values of c. The parameter values are $\Gamma/m = 10^{-2}$,

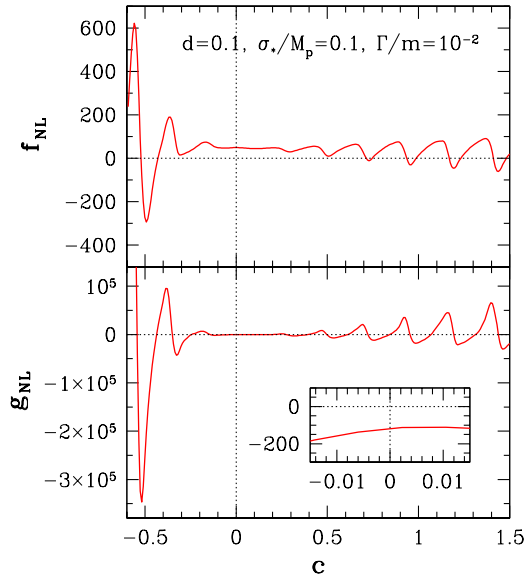

FIG. 6 (color online). $f_{\rm NL}$ and $g_{\rm NL}$ are shown as functions of c for the single-feature potential, with d, Γ/m, and σ_*/M_p kept fixed.

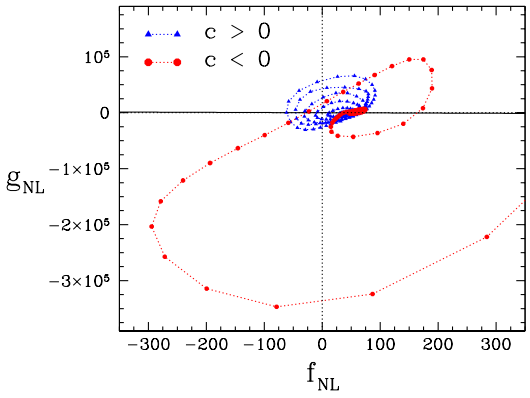

FIG. 7 (color online). $g_{\rm NL}$ versus $f_{\rm NL}$ at different values of c for the single-feature potential. The other parameter values are $\Gamma/m = 10^{-2}$, $\sigma_*/M_p = 0.1$, and $d = 0.1$.

$\sigma_*/M_p = 0.1$, and $d = 0.1$. The triangles and dots represent c values at which $g_{\rm NL}$ versus $f_{\rm NL}$ have been calculated. As can be seen from the figure, the relation between $g_{\rm NL}$ versus $f_{\rm NL}$ is scattered about the quadratic expectation. The scatter is a consequence of the fact that the phase of $g_{\rm NL}$ is slightly shifted from that of $f_{\rm NL}$.

IV. CONCLUSION AND DISCUSSION

We have studied two new curvaton models in this paper. The first is the washboard model, where the potential has tiny oscillations superimposed on the quadratic form, and the second one has a potential with two quadratic regimes having different mass scales separated by either a bump or a flattening of the potential. For the washboard model, we have investigated in detail how the two parameters that control the oscillations—namely, the amplitude and the frequency—affect the nonlinear corrections to the curvature perturbation via their effect on $f_{\rm NL}$ and $g_{\rm NL}$. We have shown that the relation $g_{\rm NL} \propto -f_{\rm NL}$, which holds for the quadratic potential, is no longer valid in this case. Rather, we find that $g_{\rm NL} \propto f_{\rm NL}$, roughly. We also found that there is a wide range of both positive and negative values for $f_{\rm NL}$, while $g_{\rm NL}$ remains negative, but its magnitude can be very large depending on the model parameters. In comparison, the quadratic potential restricts $f_{\rm NL}$ to be positive and $g_{\rm NL}$ to be negative. Moreover, we find that this model can have a large running of $f_{\rm NL}$.

For the single-feature model, we have again calculated $f_{\rm NL}$ and $g_{\rm NL}$ and demonstrated that they strongly depend on the strength of the feature and oscillate as the strength increases, with a phase shift between the two. The running of $f_{\rm NL}$ is small, in this case. The behavior of $f_{\rm NL}$ and $g_{\rm NL}$ is similar to the results of [13], where they discuss potentials with a transition from higher-order terms to a quadratic one.

What is new in the models considered here is that the curvaton motion as it oscillates about the potential minimum is nonlinear, unlike other models that have been considered so far in the literature. The results that we have found have interesting implications for searches for non-Gaussianity in observational data. The fact that $f_{\rm NL}$ can switch sign at some parameter values implies that it is possible that the nonlinear contributions to the curvature perturbation could be coming from $g_{\rm NL}$ alone, with $f_{\rm NL}$ being close to zero. A similar result was obtained in [14] in the context of the curvaton potential with nonlinear corrections to the quadratic term. It is also possible that both $f_{\rm NL}$ and $g_{\rm NL}$ contribute comparably with the same or opposite signs. The present work, thus, throws up the need to understand different sources of primordial non-Gaussianity and how they can be distinguished in the observational data. It is important to devise observables that can distinguish them. Such studies have been initiated in [41,42]. We also want to mention that $f_{\rm NL}$ and $g_{\rm NL}$ are controlled by two independent geometric quantities that characterize the hyper-surface in field space, on which multifield inflation ends. This has the implication that all of the possible results for $f_{\rm NL}$ and $g_{\rm NL}$ in curvaton models can be realized by tuning these two independent geometric quantities, as shown in [43–45].

In principle, the three free parameters in the washboard model, Γ/m, ϵ, and δ, can be constrained by using the observational constraints on $f_{\rm NL}$, $g_{\rm NL}$, and the amplitude of perturbations. The parameters c and d in the single-feature model can be similarly constrained. However, such a full scan of the parameter space is beyond the scope of the present analysis. Our purpose in this paper has been to understand the systematic behaviors of $f_{\rm NL}$ and $g_{\rm NL}$ as functions of the model parameters. We will tackle the problem of scanning the parameter space in a future work.

ACKNOWLEDGMENTS

P. C. is supported by the National Research Foundation of Korea (NRF), funded by the Korean government (MEST) (Grant No. 2009-0062868). Q. G. H. is supported by the Knowledge Innovation Program of the Chinese Academy of Sciences under the National Science Foundation of China (Grant No. 10975167. The numerical calculation in this work was carried out on the QUEST cluster computing facility at the Korea Institute for Advanced Study.

APPENDIX: CURVATON MODEL WITH QUADRATIC POTENTIAL

For the curvaton model with quadratic potential, from [40], we have

$$f_{\rm NL} = \frac{5}{4f_D} - \frac{5}{3} - \frac{5}{6}f_D, \tag{A1}$$

$$g_{\rm NL} = -\frac{25}{6f_D} + \frac{25}{108} + \frac{125}{27}f_D + \frac{25}{18}f_D^2, \tag{A2}$$

where

$$f_D = \frac{3\Omega_{\sigma,D}}{4 - \Omega_{\sigma,D}}. \tag{A3}$$

After inflation, the Universe is dominated by radiation, and the Hubble parameter is related to the cosmic time t by $H = \frac{1}{2t}$. The equation of motion of the curvaton field with quadratic potential becomes

$$\tilde{\sigma}'' + \frac{3}{2x}\tilde{\sigma}' + \tilde{\sigma} = 0, \tag{A4}$$

whose solution is

$$\tilde{\sigma} = 2^{1/4}\Gamma(5/4)x^{-1/4}J_{1/4}(x), \tag{A5}$$

where $J_\nu(x)$ is the Bessel function of the first kind. Therefore, the energy density of the curvaton is given by

$$\rho_\sigma = \frac{1}{2}m^2\sigma_*^2\left[\tilde{\sigma}^2 + \left(\frac{d\tilde{\sigma}}{dx}\right)^2\right] = \frac{\Gamma^2(5/4)}{\sqrt{2}}m^2\sigma_*^2x^{-1/2}[J_{1/4}^2(x) + J_{5/4}^2(x)]. \tag{A6}$$

Adopting the sudden decay approximation, we have

$$\Omega_{\sigma,D} = \frac{\rho_\sigma(x_D)}{3M_p^2\Gamma_\sigma^2} \simeq 0.35\frac{\sigma_*^2}{M_p^2}\sqrt{\frac{m}{\Gamma_\sigma}}, \tag{A7}$$

in the limit of $x_D = \frac{1}{2}\frac{m}{\Gamma_\sigma} \gg 1$. In the literature, $\Omega_{\sigma,D} = \frac{\sigma_*^2}{6M_p^2}\sqrt{\frac{m}{\Gamma_\sigma}}$, which is roughly half of our exact result.

[1] A. H. Guth, Phys. Rev. D **23**, 347 (1981).
[2] A. H. Guth and S. Y. Pi, Phys. Rev. Lett. **49**, 1110 (1982).
[3] K. Enqvist and M. S. Sloth, Nucl. Phys. **B626**, 395 (2002).
[4] D. H. Lyth and D. Wands, Phys. Lett. B **524**, 5 (2002).
[5] T. Moroi and T. Takahashi, Phys. Lett. B **522**, 215 (2001); **539**, 303(E) (2002).
[6] E. Komatsu *et al.*, Astrophys. J. Suppl. Ser. **192**, 18 (2011).
[7] V. Desjacques and U. Seljak, Phys. Rev. D **81**, 023006 (2010).
[8] J. Smidt, A. Amblard, A. Cooray, A. Heavens, D. Munshi, and P. Serra, arXiv:1001.5026.
[9] Q. G. Huang, Phys. Lett. B **669**, 260 (2008).
[10] Q. G. Huang, J. Cosmol. Astropart. Phys. 11 (2008) 005.
[11] K. Enqvist, S. Nurmi, G. Rigopoulos, O. Taanila, and T. Takahashi, J. Cosmol. Astropart. Phys. 11 (2009) 003.
[12] K. Enqvist and T. Takahashi, J. Cosmol. Astropart. Phys. 12 (2009) 001.
[13] K. Enqvist, S. Nurmi, O. Taanila, and T. Takahashi, J. Cosmol. Astropart. Phys. 04 (2010) 009.
[14] K. Enqvist and S. Nurmi, J. Cosmol. Astropart. Phys. 10 (2005) 013.
[15] M. Sasaki, J. Valiviita, and D. Wands, Phys. Rev. D **74**, 103003 (2006).
[16] K. Enqvist and T. Takahashi, J. Cosmol. Astropart. Phys. 09 (2008) 012.
[17] Q. G. Huang and Y. Wang, J. Cosmol. Astropart. Phys. 09 (2008) 025.
[18] M. Kawasaki, K. Nakayama, and F. Takahashi, J. Cosmol. Astropart. Phys. 01 (2009) 026.
[19] P. Chingangbam and Q. G. Huang, J. Cosmol. Astropart. Phys. 04 (2009) 031.
[20] H. Assadullahi, J. Valiviita, and D. Wands, Phys. Rev. D **76**, 103003 (2007).
[21] Q. G. Huang, J. Cosmol. Astropart. Phys. 09 (2008) 017.
[22] C. T. Byrnes, S. Nurmi, G. Tasinato, and D. Wands, J. Cosmol. Astropart. Phys. 02 (2010) 034.
[23] C. T. Byrnes, M. Gerstenlauer, S. Nurmi, G. Tasinato, and D. Wands, J. Cosmol. Astropart. Phys. 10 (2010) 004.
[24] C. T. Byrnes, K. Enqvist, and T. Takahashi, J. Cosmol. Astropart. Phys. 09 (2010) 026.
[25] Q. G. Huang, arXiv:1009.3326 [J. Cosmol. Astropart. Phys. (to be published)].
[26] Planck Collaboration arXiv:astro-ph/0604069.
[27] D. Baumann *et al.* (CMBPol Study Team Collaboration), in *CMBPol Mission Concept Study: Probing Inflation with CMB Polarization*, AIP Conf. Proc. No. 1141 (AIP, New York, 2009).
[28] E. Sefusatti, M. Liguori, A. P. S. Yadav, M. G. Jackson, and E. Pajer, J. Cosmol. Astropart. Phys. 12 (2009) 022.
[29] E. Kawakami, M. Kawasaki, K. Nakayama, and F. Takahashi, J. Cosmol. Astropart. Phys. 09 (2009) 002.

[30] T. Matsuda, Phys. Lett. B **682**, 163 (2009).
[31] T. Takahashi, M. Yamaguchi, and S. Yokoyama, Phys. Rev. D **80**, 063524 (2009).
[32] K. Nakayama and J. Yokoyama, J. Cosmol. Astropart. Phys. 01 (2010) 010.
[33] M. Kawasaki, T. Takahashi, and S. Yokoyama, J. Cosmol. Astropart. Phys. 12 (2009) 012.
[34] Y. F. Cai and Y. Wang, Phys. Rev. D **82**, 123501 (2010).
[35] J. A. Adams, G. G. Ross, and S. Sarkar, Nucl. Phys. **B503**, 405 (1997).
[36] A. A. Starobinsky, JETP Lett. **42**, 152 (1985).
[37] M. Sasaki and E. D. Stewart, Prog. Theor. Phys. **95**, 71 (1996).
[38] M. Sasaki and T. Tanaka, Prog. Theor. Phys. **99**, 763 (1998).
[39] D. H. Lyth, K. A. Malik, and M. Sasaki, J. Cosmol. Astropart. Phys. 05 (2005) 004.
[40] D. H. Lyth and Y. Rodriguez, Phys. Rev. Lett. **95**, 121302 (2005).
[41] P. Chingangbam and C. Park, J. Cosmol. Astropart. Phys. 12 (2009) 019.
[42] T. Matsubara, Phys. Rev. D **81**, 083505 (2010).
[43] Q. G. Huang, J. Cosmol. Astropart. Phys. 06 (2009) 035.
[44] M. Sasaki, Prog. Theor. Phys. **120**, 159 (2008).
[45] Q. G. Huang, J. Cosmol. Astropart. Phys. 05 (2009) 005.